Symmetry-restored Skyrme SV density functional theory

Recommended values for neutrinoless double-beta decay nuclear matrix elements

Jan Miśkiewicz
Faculty of Physics | University of Warsaw

July 1 2026, Seattle

Outline of the presentation

I. Motivation

$$2\nu\beta\beta \quad \longleftrightarrow \quad 0\nu\beta\beta$$

$2\nu\beta\beta$

- observed second-order weak process
- tests nuclear-structure models
- rarest type of radioactivity (so far)

$0\nu\beta\beta$

- forbidden in the Standard Model
- probes lepton-number violation
- requires reliable nuclear matrix elements

Same nuclei, related correlations, different operators.

I. $0\nu\beta\beta$ sensitivity

$0\nu\beta\beta$ is known to be sensitive to:

- parent-daughter nuclear deformation mismatch $\rightarrow$ good niche for **DFT-based frameworks**
- pairing correlations
- approximations used

II. Nuclear DFT in brief

1. Kohn–Hohenberg theorem:
   (a) ground state determined by density $\rho(\vec{\boldsymbol{r}}) \Longleftrightarrow |\Psi_0\rangle$
   (b) ground-state energy from a density functional $E_0 = \min_{\rho(\vec{r})} E[\rho(\vec{r})]$

2. Nuclear energy density functional:

$$E[\rho] = \int \left(\mathcal{E}_{\rm kin}[\rho] + \mathcal{E}_{\rm Coul}[\rho] + \mathcal{E}_{\rm strong}[\rho]\right) d\vec{r}. \tag{1}$$

Various forms of $\mathcal{E}_{\rm strong}$: Gogny, Skyrme, relativistic ...

$$\rho(\vec{r}) \xrightarrow{\text{minimize } E[\rho]} \rho_0(\vec{r}),\ E_0$$

In practice, nuclear EDFs depend on several local densities; here only the basic variational structure.

Generator of the Skyrme **SV** functional (also called force):

$$
\begin{aligned}
\mathcal{V}_{12}^{\mathrm{Sk}}(\mathbf{x}_1,\mathbf{x}_2) = {} & t_0(1+x_0\hat{P}_\sigma)\delta(\mathbf{r}_1-\mathbf{r}_2) \\
& + \frac{1}{2}t_1(1+x_1\hat{P}_\sigma)\left[\hat{\mathbf{k}}'^2\delta(\mathbf{r}_1-\mathbf{r}_2)+\delta(\mathbf{r}_1-\mathbf{r}_2)\hat{\mathbf{k}}^2\right] \\
& + t_2(1+x_2\hat{P}_\sigma)\hat{\mathbf{k}}'\cdot\delta(\mathbf{r}_1-\mathbf{r}_2)\hat{\mathbf{k}} \\
& + \frac{1}{6}t_3(1+x_3\hat{P}_\sigma)\rho^\alpha\left(\frac{\mathbf{r}_1+\mathbf{r}_2}{2}\right)\delta(\mathbf{r}_1-\mathbf{r}_2) \\
& + iW_0(\hat{\boldsymbol{\sigma}}_1+\hat{\boldsymbol{\sigma}}_2)\cdot\left[\hat{\mathbf{k}}'\times\delta(\mathbf{r}_1-\mathbf{r}_2)\hat{\mathbf{k}}\right].
\end{aligned}
\tag{2}
$$

The only **ρ-independent parametrization** $\rightarrow$ no singularities during I/T-projection.

II. Self-consistency

W. Kohn suggested expressing $\rho(\vec{r})$ in terms of single-particle (Kohn-Sham) orbitals:

$$\rho(\vec{r}) = \sum_{i}^{a} |\phi_i^{\mathsf{KS}}(\vec{r})|^2 \tag{3}$$

and solving for them and density ρ via Kohn-Sham-like equation:

$$\hat{h}_i^{\mathsf{KS}}(\rho)\phi_i^{\mathsf{KS}}(\vec{r}) = \epsilon^{\mathsf{KS}}\phi_i^{\mathsf{KS}}(\vec{r}). \tag{4}$$

The Hamiltonian $\hat{H} = \sum_i \hat{h}_i^{\mathsf{KS}}$ is obtained (in simple words) by functional derivative of the energy functional:

$$\hat{h}_i^{\mathsf{KS}} = \frac{\delta E[\rho]}{\delta \rho_{ij}}. \tag{5}$$

The self-consistency is reached, when in the n^{th} iteration stability of ρ, ϕ_i and other observables (E, Q_2, ...) is obtained within given precision ε.

II. Skyrme SV functional

- Fault: low effective mass m^* makes pairing interaction ineffective if parity of a nucleon changed.

- Advantage: density-independence makes projection safe from running into singularities.

III. Projection on good angular momentum and isospin

The good quantum numbers are restored by averaging mean-field rotated intrinsic states $|\psi\rangle$ over angles in space (I-restoration) or isospace (T-restoration):

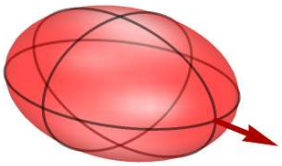

Figure 1: Intrinsic frame.

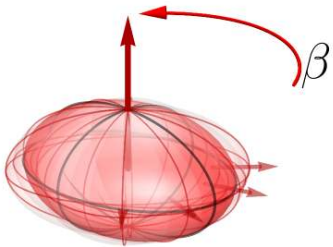

Figure 2: Laboratory frame.

Mathematically, we apply rotational symmetry operator

$$|\psi(\Omega)\rangle = e^{i\alpha\hat{J}_z} e^{i\beta\hat{J}_y} e^{i\gamma\hat{J}_z} |\psi\rangle \tag{6}$$

integrate it with $\mathcal{D}$-Wigner function as weight:

$$|\psi; IMK; T_z\rangle = \frac{2I+1}{8\pi^2} \int \mathcal{D}^{*I}_{MK} |\psi(\Omega)\rangle \; d\Omega = \hat{P}^I_{MK} |\psi\rangle \tag{7}$$

and mix within K-quantum number:

$$|\psi; IM; T_z\rangle = \frac{1}{\sqrt{\mathcal{N}_{\psi;IM;T_z}}} \sum_K a_K \hat{P}^I_{MK} |\psi\rangle. \tag{8}$$

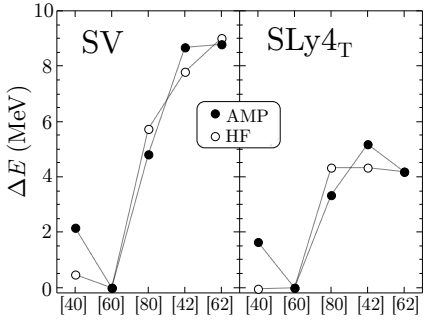

Figure 3: Intrinsic (HF) vs projected (AMP) energies in ^{76}Ge. $[n, m]$ denotes respectively neutronic and protonic occupation of $0g_{9/2}$ orbital.

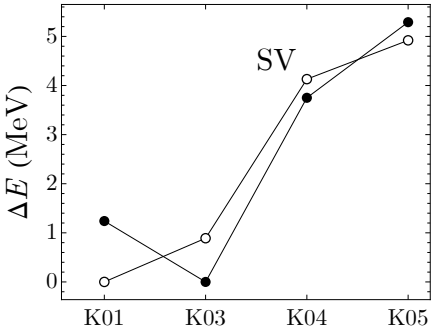

Figure 4: Intrinsic (HF) vs projected (AMP) energies in ^{100}Ru.

III. DFT–NCCI realization

Skyrme SV density functional

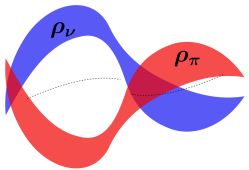

$\frac{\delta}{\delta\rho}$

Slater determinant mean field

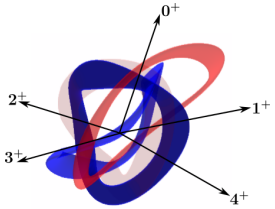

no good quantum numbers

~~γ, β transitions~~

$I(T)$-projection

Hill–Wheeler

NCCI basis

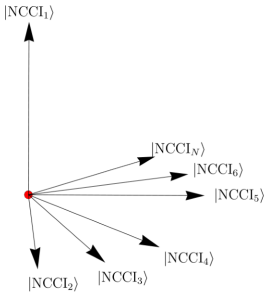

good quantum numbers

γ, β transitions

DFT | **DFT-NCCI**

III. No Core framework

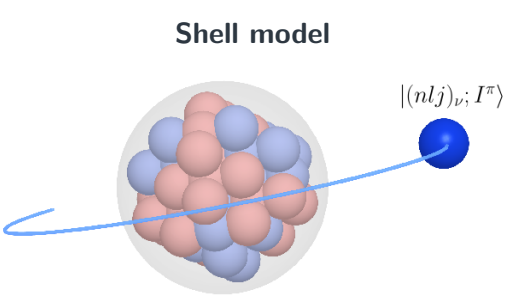

Figure 5: Configurations built on a closed-shell inert core.

- configurations built on a closed-shell inert core
- valence nucleons coupled to good angular momentum I
- good quantum numbers imposed

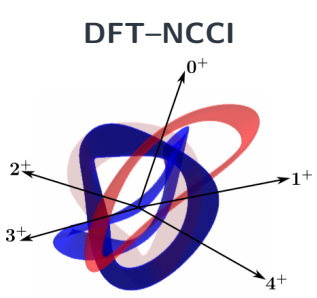

Figure 6: No inert core: all nucleons enter the self-consistent Slater determinant.

- no inert core
- self-consistent Slater determinants of all nucleons
- good angular momentum I restored by projection

III. Superallowed Fermi beta decay in DFT-NCCI

Master thesis of J.Wysocki (2025) from Warsaw nuclear group: evaluation of isospin-symmetry-breaking correction δ_C for $^{10}\mathrm{C} \rightarrow ^{10}$ B superallowed Fermi beta decay.

$$\mathcal{F}t := ft(1 + \delta'_R)(1 + \delta_{NS} - \delta_C)$$

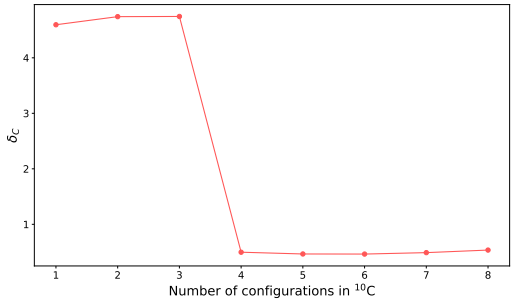

Figure 7: Convergence of δ_C with parent configurations. Values in %.

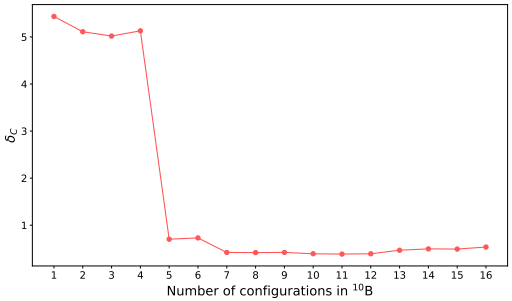

Figure 8: Convergence of δ_C with daughter configurations. Values in %.

IV. Generalized Wick's Theorem

The matrix elements between I-projected Slater determinants $|\varphi; I'M'K'\rangle$ and $|\psi; IMK\rangle$ can then be written as:

$$\begin{aligned}\mathcal{M}^{\mathrm{GT}}_{\mu\nu} &= \langle\varphi; I'M'K'; T_z - 1|\hat{\mathcal{O}}^{\mathrm{GT}}_{\mu\nu}|\psi; IMK; T_z\rangle \\ &= C^{I'M'}_{IM,\,1\nu} \sum_{\xi} C^{I'K'}_{I\,K'-\xi,\,1\xi} \frac{2I+1}{8\pi^2} \int d\Omega\, D^{I*}_{K'-\xi,\,K}(\Omega) \\ &\quad \times \langle\varphi|\hat{\tau}_{1\mu}\,\hat{\sigma}_{1\xi}|\widetilde{\psi}\rangle,\end{aligned} \tag{9}$$

where $|\widetilde{\psi}\rangle \equiv \hat{R}(\Omega)|\psi\rangle$ denotes the rotated Slater determinant.

IV. Generalized Wick's Theorem

The resulting matrix element between I-projected states may be translated into one-body transition densities $\boldsymbol{\rho}$:

$$\langle\psi_r|\hat{\tau}_{1\eta}\hat{\sigma}_{1\xi}|\widetilde{\psi}\rangle = \langle\psi(T_z-1)|\widetilde{\psi}(T_z)\rangle \int d\mathbf{r} \sum_{qq';\,\sigma\sigma'} \langle q|\hat{\tau}_{1\eta}|q'\rangle\langle\sigma|\hat{\sigma}_{1\xi}|\sigma'\rangle\widetilde{\boldsymbol{\rho}}(\mathbf{r}\sigma' q';\mathbf{r}\sigma q). \tag{10}$$

Note that the overlap $\langle\varphi(T_z-1)|\psi(T_z)\rangle \propto \delta_{T_z,T_z-1} = 0 \longrightarrow$ **ORTHOGONAL!**

IV. Workaround: rotation in isospin

We can restore non-zero overlap by performing an additional rotation in isospin space of one Slater determinant, which aligns the isospin projections.

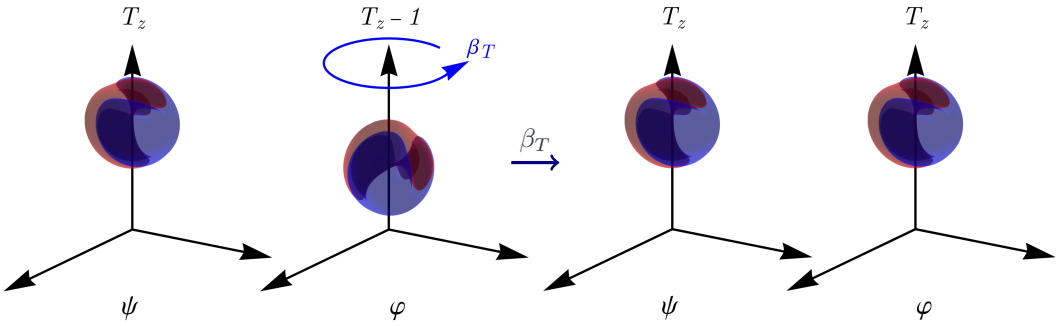

Figure 9: Additional rotation in isospin space.

This procedure introduces an additional integration over the isospin angle β_T.

Results for $2\nu\beta\beta$

V. A48: Configuration classes

^{48}Ca (parent)

1. Seniority-zero nn-pairs

24
configurations

^{48}Sc (virtual)

1. Seniority-two in $f_{7/2}$
2. Single n-excitations across $N = 28$
3. Single p-excitations across $Z = 28$

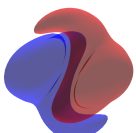

54
configurations

^{48}Ti (daughter)

1. Seniority-zero nn- and pp-pairs in $f_{7/2}$
2. np-pairing in $f_{7/2}$
3. Seniority-zero nn-pairs across $N = 28$ shell
4. Seniority-zero pp-pairs across $Z = 28$ shell

49
configurations

V. A48: Convergence

No single-state dominance: many small partial NMEs build **88**% of the total value.

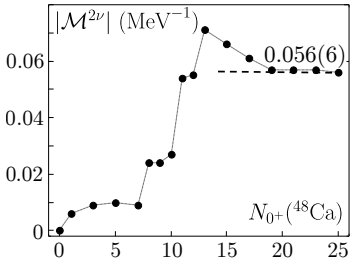

Figure 10: $\mathcal{M}^{2\nu}$ convergence wrt ^{48}Ca configuration space.

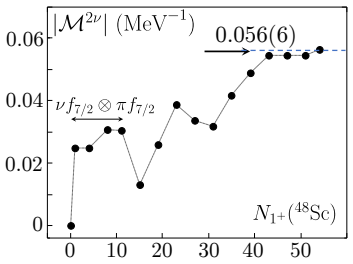

Figure 11: $\mathcal{M}^{2\nu}$ convergence wrt ^{48}Sc configuration space.

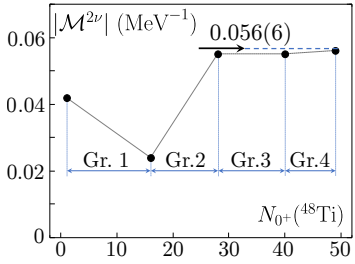

Figure 12: $\mathcal{M}^{2\nu}$ convergence wrt ^{48}Ti configuration space.

V. A48: Comparison with other models

Reference	Method	$\lvert\mathcal{M}^{2\nu}\rvert$ (MeV^{-1})
A. S. Barabash (2020)	Experiment	0.068 ± 0.006
Y. Iwata et al. (2015)	Shell model	0.0539
F. Šimkovic et al. (2018)	ChER	0.0832
J. Kostensalo and J. Suhonen (2019)	Shell model	0.100
S. Novario et al. (2021)	Coupled cluster	0.082
J. Terasaki and Y. Iwata (2021)	Shell model	0.0515
	QRPA	0.0745
P. Veselý et al. (2024)	STDA	0.1668
J. Miśkiewicz, M. Konieczka and W. Satuła (2025)	**DFT-NCCI**	$\mathbf{0.056}$

Comparison of DFT-NCCI matrix element magnitude with other nuclear models. Values for other models converted from dimensionless units to MeV^{-1} assuming $g_A = 1$.

For more details see: **Phys. Rev. C, 112:055502, 2025**.

V. A76: Skyrme SV induced decay paths

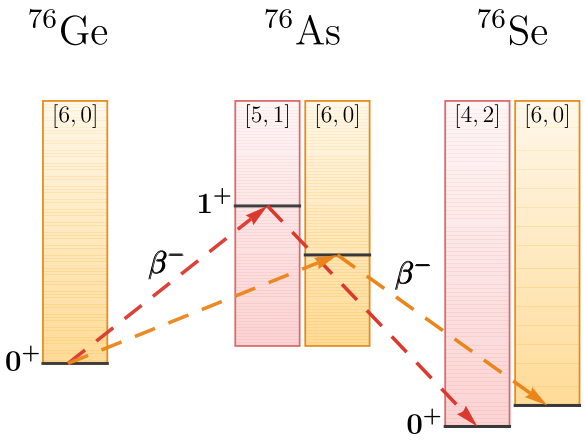

Virtual transitions split into two, nonmixing paths of different $[\nu, \pi]$ $0g_{9/2}$ orbital occupation. Red/orange levels denote active orbitals of positive/negative parity.

Figure 13: Two paths of different parity structure: C42 (positive, red) and C60 (negative, orange).

V. A76: C42 path (positive parity)

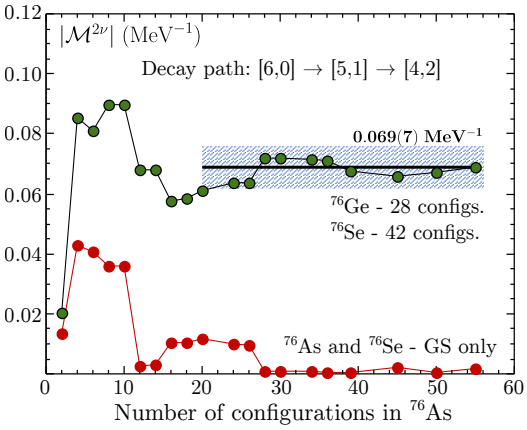

Figure 14: Stability of the $|\mathcal{M}^{2\nu}|$ matrix element as a function of the number n of configurations in the virtual nucleus ^{76}As.

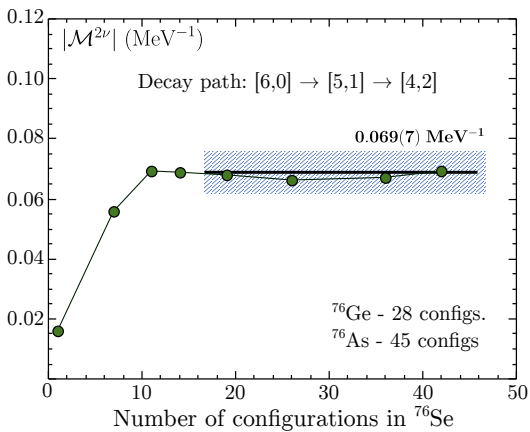

Figure 15: Stability of the $|\mathcal{M}^{2\nu}|$ matrix element as a function of the number n of configurations in the daughter nucleus ^{76}Se.

V. A76: C42 path summary

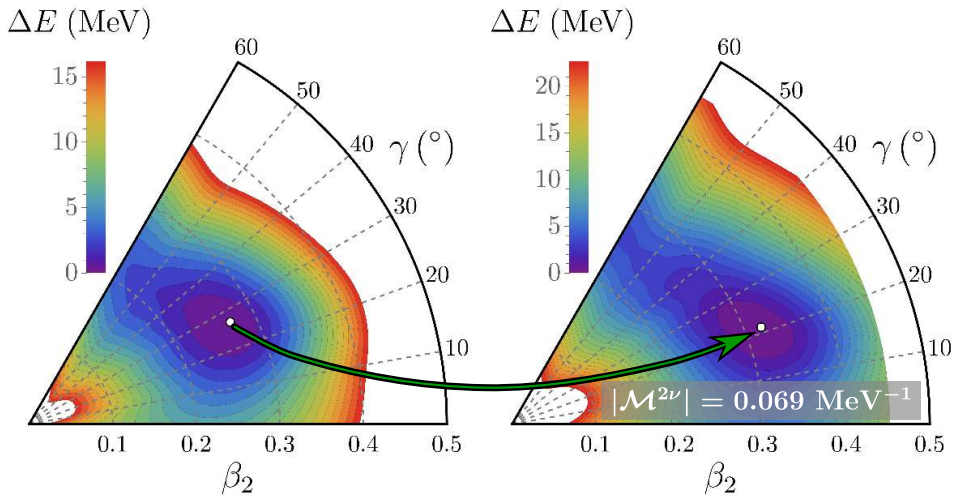

Figure 16: Dominant C42 path between the lowest-energy minima.

V. A76: Shape coexistence in daughter nucleus

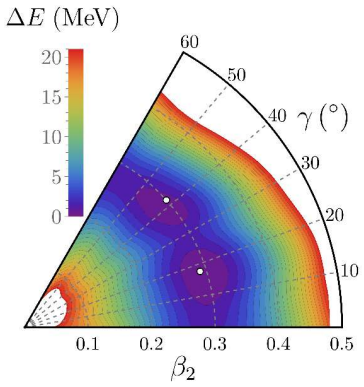

Figure 17: Shape coexistence in the ^{76}Se $[6, 0]$.

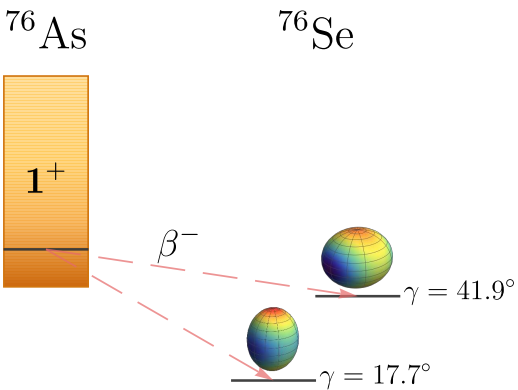

Figure 18: Two coexisting minima act as distinct final state candidates and give rise to different values of the $2\nu\beta\beta$ nuclear matrix element.

V. A76: C60 path (negative parity)

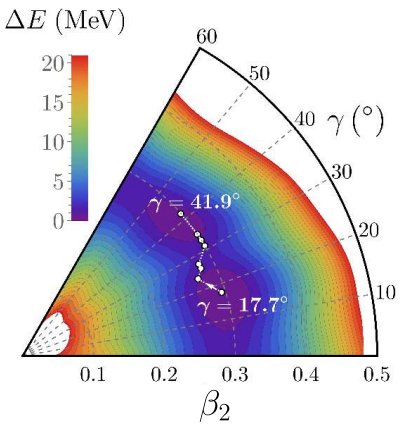

Figure 19: Correlating two different minima in ^{76}Se via vibrational states constructed on the Q_2-barrier.

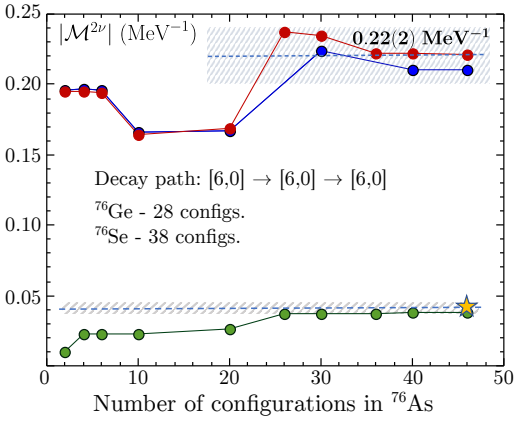

Figure 20: Green: $\gamma = 17.7°$ minimum. Black/red: uncorrelated/correlated $\gamma = 41.9°$ minimum. Star: Q_2-barrier states in ^{76}Se.

V. A76: C60 path summary

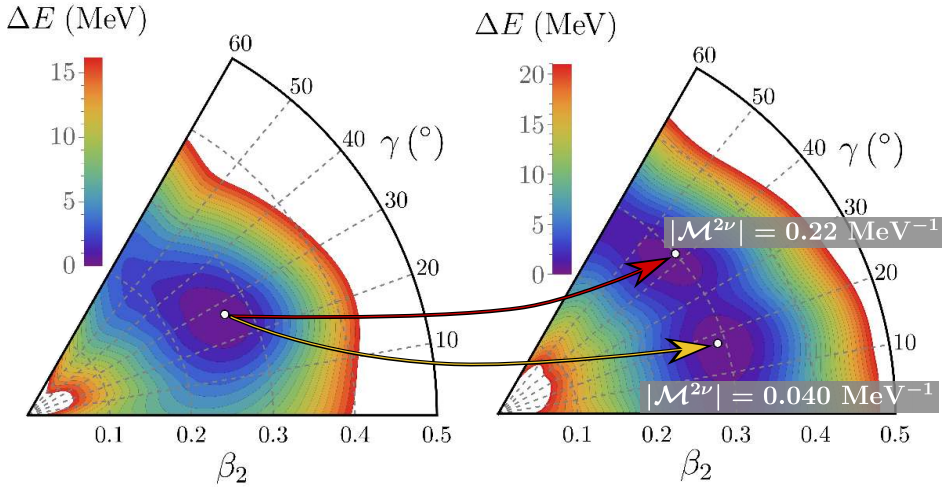

Figure 21: C60 path: competing minima lead to distinct matrix elements.

V. A76: Comparison with other models

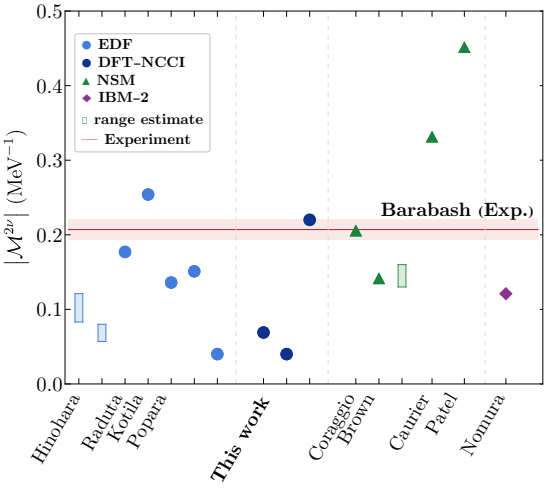

Figure 22: A summary of selected NME calculated using different models.

All values are renormalized to the effective axial-vector coupling constant $g_{\mathrm{A}}^{(\mathrm{eff})} = 1$. For other details see **arXiv:2605.14813** (currently in review in PRC).

V. A100: Similar story to A76?

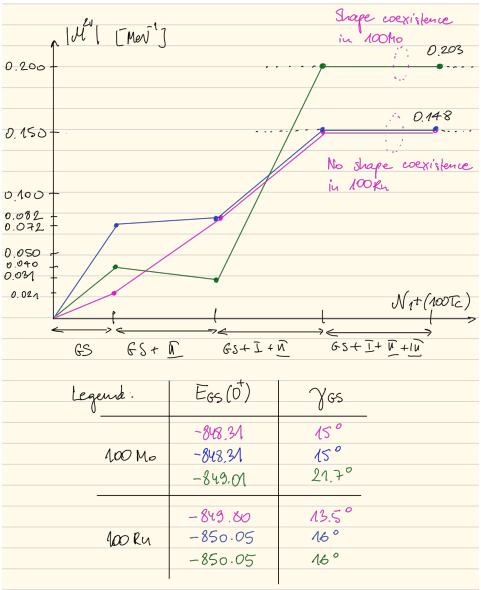

Legend:	$E_{GS}(0^+)$	γ_{GS}
	-848.31	15°
100 Mo	-848.31	15°
	-849.01	21.7°
	-849.80	13.5°
100 Ru	-850.05	16°
	-850.05	16°

PRELIMINARY

- 3 classes of virtual configurations in ^{100}Tc: ν(1p-1h)$_{g7/2}$, π(1p-1h)$_{g9/2}$ and π(1p-1h)$_{g7/2}$.
- Two coexisting minima observed in parent ^{100}Mo.
- Single minimum in daughter ^{100}Ru.
- Resulting $\mathcal{M}^{2\nu}$ dependent on the ^{100}Mo triaxiality.
- Correlation of parent and daughter still to be explored.

VI. Plans for $0\nu\beta\beta$

- First attempt: closure approximation.
- Expressing closure matrix elements in HFODD numerical code

$$\hat{\mathcal{O}}_{\mathsf{F}} = \tau_1^- \tau_2^- H_{\mathsf{F}}\big(r, \langle E \rangle\big), \tag{11}$$

$$\hat{\mathcal{O}}_{\mathsf{GT}} = \tau_1^- \tau_2^- (\vec{\sigma}_1 \cdot \vec{\sigma}_2) H_{\mathsf{GT}}\big(r, \langle E \rangle\big). \tag{12}$$

  in terms of one-body transition densities:

$$\mathcal{M}_\alpha^{0\nu} \sim H_\alpha(\langle E \rangle) \sum_{\mu\nu\lambda\pi} \bar{\mathcal{O}}^\alpha_{\mu\nu\lambda\pi} \tilde{\rho}_{\mu\nu} \tilde{\rho}_{\lambda\pi}, \qquad \alpha \in \{\mathrm{F}, \mathrm{GT}\}. \tag{13}$$

- Generalized Wick's Theorem should work for $T_z \to T_z - 2$.

Summary

- Skyrme SV enables symmetry restoration without density-dependent projection singularities.
- DFT–NCCI provides no-core, projected many-body states with good I and T.
- $2\nu\beta\beta$ results show strong sensitivity to configuration mixing and shape coexistence.
- Extension to $0\nu\beta\beta$ is planned through closure matrix elements and transition densities.